

See discussions, stats, and author profiles for this publication at: <https://www.researchgate.net/publication/231646852>

Stability of Nanodiamond Surfaces Exposed to N, NH, and NH₂

ARTICLE *in* THE JOURNAL OF PHYSICAL CHEMISTRY C · MARCH 2011

Impact Factor: 4.77 · DOI: 10.1021/jp1111026

CITATIONS

16

READS

98

2 AUTHORS, INCLUDING:



Amanda S Barnard

The Commonwealth Scientific and Industrial...

181 PUBLICATIONS 4,317 CITATIONS

SEE PROFILE

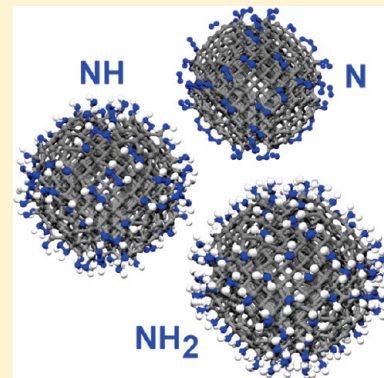
Stability of Nanodiamond Surfaces Exposed to N, NH, and NH₂

Lin Lai and Amanda S. Barnard*

CSIRO Materials Science and Engineering, Clayton, VIC, 3168, Australia

S Supporting Information

ABSTRACT: Knowledge about the surface functionalization of nanodiamonds is of great importance for nanomedical and nanobiological applications. In this paper, we explore the relative stability of the nanodiamond passivated by amidogen (NH₂), imidogen (NH), and nitrogen (N) in N₂ + H₂ and ammonia environments, using density functional tight binding simulations over a range of temperatures. The N-adsorption is found to be energetically unfavorable on the nanodiamond surfaces up to 1500 K. In contrast, adsorption of NH and NH₂ is found to be thermodynamically stable at least around room temperature. We also compare the possibility of anisotropic (facet-dependent) adsorption and find that {100} facets of the nanodiamond are more preferred for the NH adsorption in the entire temperature range considered but are only favored at high temperature for the NH₂ adsorption. We also show that this chemical functionalization is more stable in the N₂ + H₂ environment than in the ammonia environment, but its stability depends on the size, shape, and morphology of the nanodiamond.



INTRODUCTION

Nanodiamonds^{1–3} are unique structures with electronic properties that depend upon their size and morphology,⁴ which makes them a candidate component for optoelectronic devices,⁵ composites,⁶ and new emerging applications in biotechnology and nanomedicine.^{7,8} This has prompted numerous studies investigating aspects such as the interactions and reactivity,^{9–12} surface structure and core crystallinity,^{13–15} and the properties of defects.¹⁶ Most of the studies reported to date have concentrated on exploring the location and configuration of functional defects in the colloidal nanodiamond, including the important nitrogen-vacancy (N-V)^{17–19} and silicon-vacancy (Si-V)^{20,21} defects, which are optically active in the visible spectrum. The strong fluorescence of the N-V defect,^{22,23} combined with the lack of cytotoxicity,^{24,25} is largely responsible for the nanodiamond becoming a preferred candidate for use as a biomarker.^{26–28} This is an important complement to alternative uses for nanodiamonds in the field of drug delivery,²⁹ which confirms its status as an important multifunctional nanomaterial.³⁰

In general, the effectiveness of the nanodiamond in many biomedical applications is intrinsically linked to the location, configuration, and stability of nitrogen in a number of ways. First, the stable inclusion of nitrogen as N-V defects, as opposed to single atom dopants³¹ or interstitial impurities,³² is critical in delivering the highly desirable optical properties. Previous work has indicated that substitutional nitrogen is not thermodynamically stable within the core of the nanodiamond but prefers to occupy lattice positions at the surface, irrespective of the size of the particle.³³ This leads to speculation that N-V centers would escape the particles via vacancy-assisted diffusion,¹⁷ particularly when the nitrogen atom resided at lattice sites that fall within a

Bohr radius from the surfaces, edges, or corners.³⁴ However, when similar simulations were used to explore the stability of the N-V combination and the kinetic barriers to diffusion, it was found that the core–shell sp³/sp² structure served to trap nitrogen within the core and ensure that the probability of escape was reduced.³⁵ This all-carbon core–shell structure, known as a bucky-diamond,^{36,37} does however affect the photostability, and recent results have revealed that mobility of the donor electron gives rise to blinking when the defect is sufficiently close to the sp²-bonded shell.³⁸

In addition to this, the interaction of nitrogen groups with the surfaces of diamond nanoparticles is an important part of functionalization^{39–41} and may be attached in a number of ways.^{42–46} Proteins and other macromolecules often contain amide groups that can interact with carbon-based systems and aid in immobilization⁴⁷ and applications such as drug delivery.⁴⁸ It has previously been shown that, in the case of diamond, amine terminations show an increased potential for acting as useful intermediaries for further functionalization, as well as serving as a substrate for self-assembly of other biomolecules.^{42,49} For example, recently a new method was introduced using nanodiamonds as vectors for in vitro gene delivery via surface-immobilization with 800 Da polyethyleneimine (PEI800) and covalent conjugation with amine groups,⁵⁰ as part of a rapid, scalable, and broadly applicable gene therapy strategy. However, before we can begin to address more complex interactions between nanodiamonds and proteins and macromolecules, we

Received: November 21, 2010

Revised: February 7, 2011

Published: March 22, 2011

Table 1. Comparison of the Binding Energies (E_b) of H_2 , N_2 , and NH_3 by SCC-DFTB and DFT Calculations in Units of eV

molecules	SCC-DFTB	GGA (PBE)	GGA (BLYP)	LDA(CA-PZ)
H_2	-3.42	-4.19	-4.75	-4.58
N_2	-10.02	-11.48	-10.19	-13.84
NH_3	-12.55	-13.76	-12.90	-15.86

must first ascertain how nanodiamonds and amines interact in isolation, a topic that has been largely overlooked to date.

In the present study, we have used density functional tight binding computer simulations to investigate the stability of diamond nanoparticles passivated with amine groups, in comparison to different nitrogen-rich environments. We have included primary amine (NH_2 , amidogen), secondary amine (NH , imidogen), and tertiary amine (N , atomic nitrogen) and have selectively and systematically applied monolayers to different crystal facets on model particles. Our results show that passivation with nitrogen is thermodynamically unfavorable, and spontaneous desorption from all low index facets may be expected, even at low temperature. In contrast, amidogen and imidogen form stable chemical bonds with the surface, but the relative stability depends upon the facet orientation, the temperature, and the surrounding chemical environment.

■ COMPUTATIONAL METHODS

The density functional based tight-binding method with self-consistent charges (SCC-DFTB)^{51,52} is a two-center approach to density functional theory (DFT), where the Kohn–Sham density functional is expanded to second order around a reference electron density. The reference density is obtained from self-consistent density functional calculations of weakly confined neutral atoms, and the confinement potential is optimized to anticipate the charge density and effective potential in molecules and solids. A minimal valence basis is established, and one- and two-center tight-binding matrix elements are explicitly calculated within DFT. A universal short-range repulsive potential accounts for double counting terms in the Coulomb and exchange-correlation contributions, as well as the internuclear repulsion, and self-consistency is included at the level of Mulliken charges, as described by Frauenheim and coauthors.⁵² This method has been selected for use here as it has previously been shown to be suitable for studying diamond nanoparticles.^{15,21,31,33–35,38,53,54} We have employed the pbc set of parameters⁵⁵ involving hydrogen, carbon, and nitrogen that were reported by Köhler et al.⁵⁶ These parameters have been thoroughly tested in the past; however, to provide a further comparison, the binding energies of H_2 , N_2 , and NH_3 molecules calculated with the SCC-DFTB method are shown in Table 1, where we can see they are in good agreement with results from DFT calculations.

The particles used in this study are a C_{837} truncated octahedral structure displaying six $\{100\}$ facets and eight $\{111\}$ facets and a C_{705} rhombitruncated cuboctahedron displaying six $\{100\}$ facets, eight $\{111\}$ facets, and twelve $\{110\}$ facets. These shapes have been selected for inclusion here since they are consistent with the shapes observed experimentally, while offering a range of different crystallographic facets at a size that is computationally reasonable. The rhombitruncated cuboctahedron is generated by truncating the $\{111\}|\{111\}$ edges of the truncated octahedron, and both particles adopted the bucky-diamond structure following geometric optimization in the absence of passivation (see Figure 1).

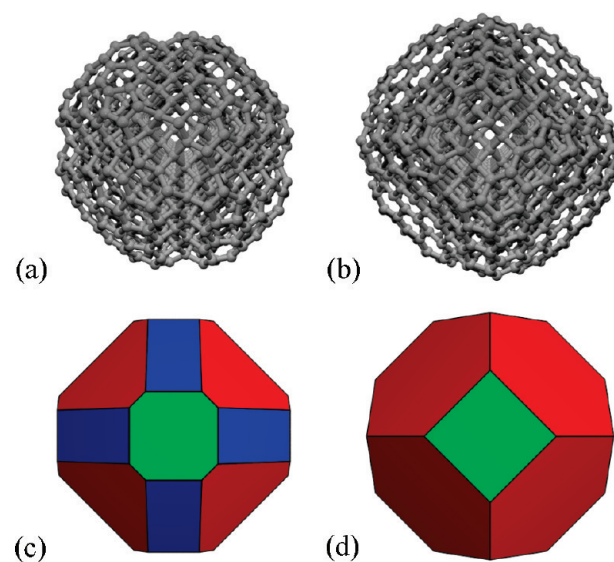


Figure 1. Fully relaxed structures of (a) C_{705} and (b) C_{837} nanodiamonds in ball and stick model (top), in which gray balls denote the C atoms. To present the geometric morphology the corresponding schematic representation of (c) C_{705} and (d) C_{837} nanodiamonds is also shown (bottom). In each case, the $\{111\}$ facets are shown in red, the $\{100\}$ facets in green, and the $\{110\}$ facets in blue.

Prior to relaxation, each of these structures was selectively chemisorbed with the N, NH, or NH_2 to determine how the adsorption behavior is related to the size and shape of the particle and more specifically to the types of surface facets. Although deliberate selective functionalization of the nanodiamond has not yet been realized experimentally, it is possible that certain groups may show a natural affinity to different facets since they exhibit distinctly different types of reconstructions. While both the $\{100\}$ and $\{110\}$ facets are decorated by 2-fold coordinated C atoms in the terminal plane (with two dangling bonds), the $\{100\}$ surface adopts a 2×1 reconstruction to reduce the number of unpaired electrons, whereas the $\{110\}$ surface forms only tilted chains and retains the gross undercoordination. The $\{111\}$ surface is decorated by 3-fold coordinated C atoms in the terminal plane but reconstructs to form a curved sp^2 -bonded fullerene structure to reduce the $\pi-\pi$ overlap. The existence (and coexistence) of these different types of surface and reconstructions makes predicting the preferred interactions with adsorbates, and the response of the remainder of the nanodiamond, a very complicated task.

To sample a full range of different types of adsorption configurations, we have selectively and systematically patterned the two model structures with monolayers of N, NH, or NH_2 . First, adsorption was restricted to single facet types, i.e., just the $\{100\}$ facets, just the $\{111\}$ facets, or (on the C_{705} particle) just the $\{110\}$ facets. This enables a comparison of which facets may offer preferential sites for amine adsorption. In addition, this adsorption was restricted from single facet types, i.e., all but the $\{100\}$ facets, all but the $\{111\}$ facets, or (on the C_{705} particle) all but the $\{110\}$ facets. This enables a comparison of which “bare” facets may offer preferential reconstructions that increase the stability of the entire structure. All of these results were compared to fully passivated structures (where a monolayer coverage was applied to all facets simultaneously) and “bare” structures (where passivation was not allowed on any facets). Following a full

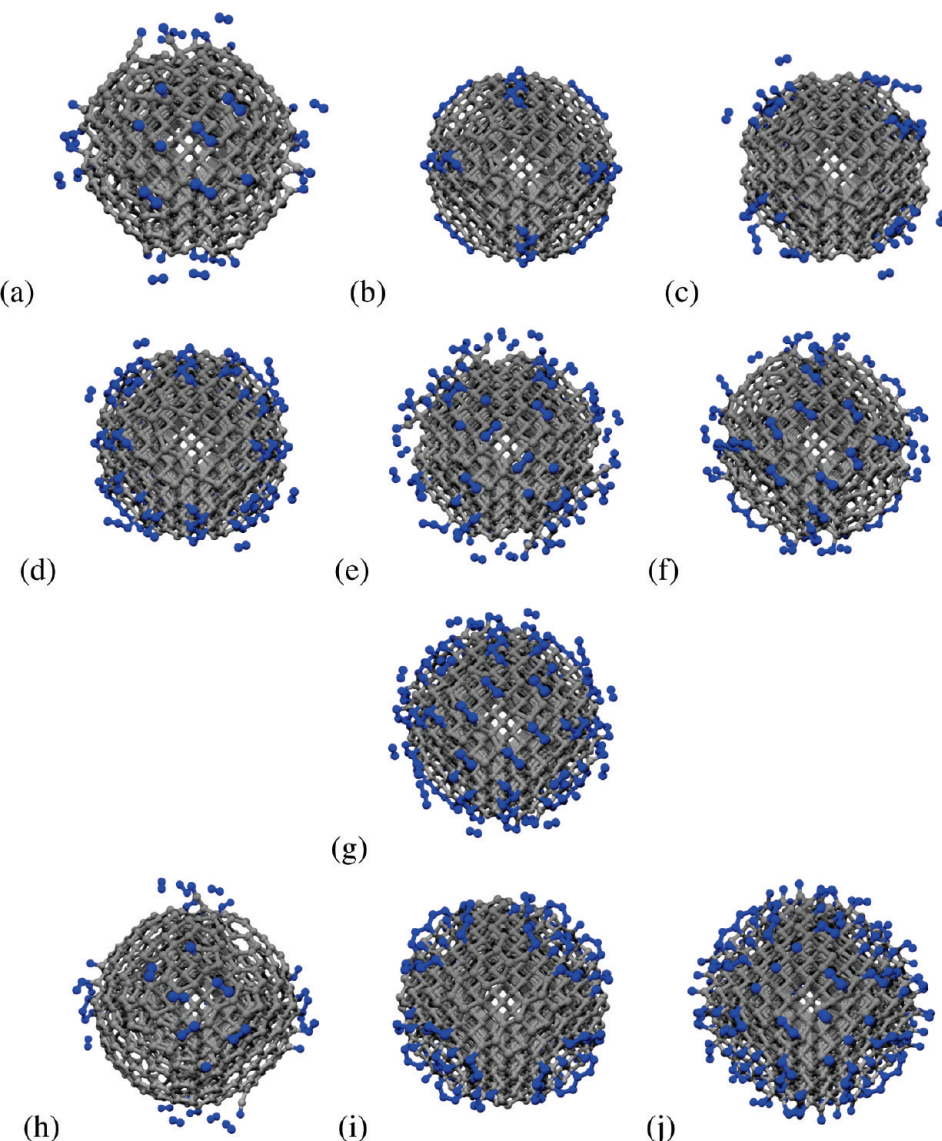


Figure 2. Fully relaxed structures for N atom adsorbing on (a) {100} facets, (b) {110} facets, (c) {111} facets, (d) {110} and {111} facets ({100} clean), (e) {100} and {111} facets ({110} clean), (f) {100} and {110} facets ({111} clean), and (g) the entire surface of the C₇₀₅ nanodiamond, and on (h) {100} facets, (i) {111} facets, and (j) the entire surface of the C₈₃₇ nanodiamond. The blue and gray balls denote the N atoms and C atoms, respectively.

geometric optimization, to a convergence of 1.0×10^{-4} a.u. ≈ 5 meV Å⁻¹, the nanodiamond–amine systems were analyzed and compared. A complete and detailed structural characterization of the final nanodiamond/amine combinations is provided in the Supporting Information.

RESULTS AND DISCUSSION

Stability. To evaluate the stability of amine-functionalized nanodiamonds, we develop a thermodynamic formalism where the formation energy per atom, E_f is defined as

$$E_f = (\mu_{ND,X} - n_C \times \mu_C - n_X \times \mu_X) / N_t \quad (1)$$

Here, $\mu_{ND,X}$ denotes the chemical potential of the nanodiamond (ND) combined with adsorbate (X) in one simulation, which is set to be equal to its static total energy. The chemical potential of the C atom, μ_C , is equal to the total energy per C

atom in clean (unpassivated), fully relaxed, equivalent structures. In this context *unpassivated* refers to the bucky-diamond structures (as shown in Figure 1), with fully reconstructed surfaces, which includes graphitization of the {111} facets. This means that the zero formation energy will represent our (bucky-diamond) frame of reference, and all calculated differences represent relative stabilities, in the absence of coarsening (mass of the ND is conserved). The n_C , n_X , and N_t represent the number of C atoms, X atoms or molecules, and atoms in the passivated nanodiamond, respectively. To generate the comparisons between different adsorption environments, we employ two thermodynamic equilibrium constraints

$$\mu_{NH_x} = \mu_N + x \times \mu_H \quad (2)$$

and

$$\mu_{NH_x} = \mu_{NH_3} - (3 - x) \times \mu_H \quad (3)$$

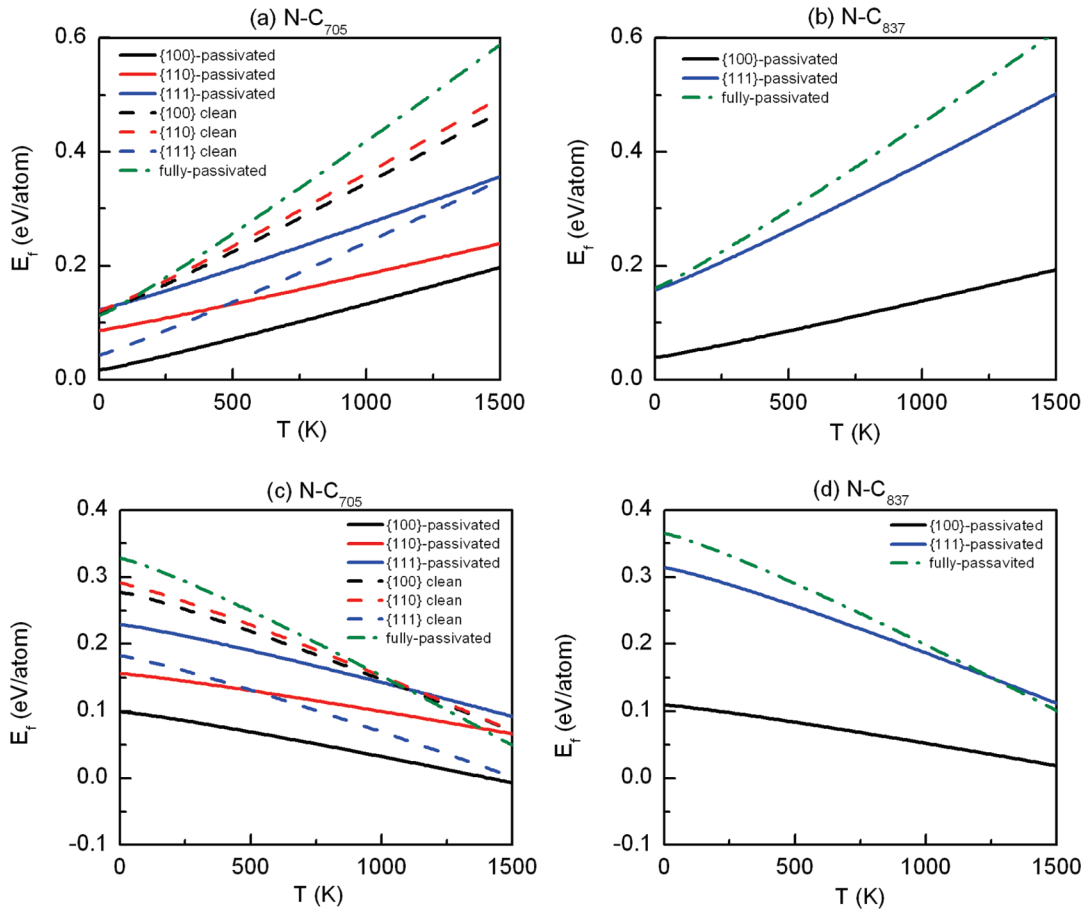


Figure 3. Formation energies in units of eV/atom, E_f , for C₇₀₅ and C₈₃₇ nanodiamonds with variant nitrogen (N) adsorption. Panels (a) and (b) are plotted with N₂ as the reservoir while panels (c) and (d) with NH₃ as the reservoir.

where x is the number of H in NH_x. The chemical potentials of N, H, and NH₃ are denoted by μ_N , μ_H , and μ_{NH_3} , respectively. These values will depend on the chemical reservoir and will be indicative of the reactants prior to adsorption or the reaction products following desorption. With nitrogen and hydrogen gas as the reservoir, eq 2 is applied. The values of μ_N and μ_H are half of the chemical potentials of N₂ and H₂ molecules, respectively. On the other hand, with ammonia gas as the reservoir, eq 3 is used. The μ_H is still equal to half of the chemical potential of H₂, while μ_N is derived from $\mu_N = \mu_{NH_3} - 3 \times \mu_H$. In both cases the chemical potential of a molecule is defined as

$$\mu_X = E_X + h\nu/2 + k_B T \ln(PV/k_B T) \quad (4)$$

In eq 4, X can be substituted by the N₂, H₂, or NH₃ molecule; E_X equals to the molecular energy; P and T are the atmospheric pressure (1 atm) and temperature, respectively; and ν is the sum of the fundamental vibrational frequencies (including symmetric/antisymmetric stretching and deformation modes) of the gas molecules used as the resources (H₂, N₂, and NH₃), which is equal to their experimental values based on gas-phase infrared, Raman, or ultraviolet spectra.⁵⁷ The rotational energy of the gas molecule in the reservoirs is ignored in this study, as they are typically around 2 orders of magnitude smaller than the vibrational contribution for such small molecules. Finally the volume V is derived from the quantum volume ($h^2/2\pi m_X k_B T$)^{3/2}, where m_X is the mass of a single N₂, H₂, or NH₃ molecule, and h and k_B are the Planck and Boltzmann

constants, respectively. In addition, we calculate the adsorption energy to characterize the functionalization ability for variant facets, which is defined as

$$E_a = (\mu_{ND,X} - n_C \times \mu_C - n_X \times \mu_X)/n_X \quad (5)$$

Nitrogen Adsorption (N). Simulation results for nitrogen adsorption are shown in Figure 2, and the formation energies for N-adsorbed C₇₀₅ and C₈₃₇ nanodiamonds in the atmosphere (N₂ and H₂ as the reservoir) and ammonia environments (NH₃ as the reservoir) are presented in Figure 3, as a function of temperature. We can see that, in general, chemisorption of N on the surfaces of the nanodiamond is endothermic in this atmosphere and that desorption is prevalent. The calculated formation energies (Figure 3a) at $T = 0$ for N on the {100}, {110}, and {111} facets of the C₇₀₅ nanoparticle are 0.02, 0.09, and 0.12 eV per atom, respectively. This indicates that, on the rhombitruncated cuboctahedral nanodiamond, forced adsorption of N on the {100} facets is more favorable than the alternative facets, but N adsorption is unstable with respect to desorption and the formation of N₂. This finding remains unchanged up to 1500 K and is further supported by the results for all other configurations.

Similarly, for the truncated octahedral C₈₃₇ nanoparticle the {100} facets are the most favorable surfaces for N adsorption (Figure 3b), but this is once again unstable with respect to

Table 2. Adsorption Energies, E_a , in Units of eV at $T = 0$ for N, NH, and NH₂ Groups Adsorbing on Variant Facets in C₇₀₅ and C₈₃₇ Nanoparticles

N-functionalization	N ^a	N ^b	NH ^a	NH ^b	NH ₂ ^a	NH ₂ ^b
C ₇₀₅ (100) surface	0.181	1.063	-1.083	-0.201	-2.874	-1.992
C ₇₀₅ (110) surface	1.102	1.984	-0.597	0.285	-1.746	-0.864
C ₇₀₅ (111) surface	1.027	1.909	-0.508	0.375	-2.397	-1.514
C ₇₀₅ (100) clean	0.648	1.531	-0.630	0.253	-2.249	-1.367
C ₇₀₅ (110) clean	0.628	1.510	-0.905	-0.023	-2.601	-1.719
C ₇₀₅ (111) clean	0.273	1.155	-0.958	-0.076	-2.588	-1.706
C ₇₀₅ fully passivated	0.460	1.342	-0.863	0.019	-2.376	-1.494
C ₈₃₇ (100) surface	0.490	1.372	-0.910	-0.028	-2.723	-1.840
C ₈₃₇ (111) surface	0.891	1.773	-0.664	0.218	-2.465	-1.583
C ₈₃₇ fully passivated	0.695	1.577	-0.863	0.019	-2.549	-1.666

^a In an atmospheric reservoir. ^b In an ammonia reservoir.

desorption and the formation of N₂. Interestingly, it is found that N adsorption is slightly less stable on certain facets of C₈₃₇ than on corresponding facets of C₇₀₅, and we find that the formation energy for the fully-N-passivated C₈₃₇ is greater than that of the fully-N-passivated C₇₀₅ nanoparticle. The probable cause is the lack of {110} facets on the truncated octahedral C₈₃₇ nanoparticle, which increases the total number of adsorption sites present on the {111} facets. The {111} facets on the C₈₃₇ particle contain a total of 180 possible adsorption sites, whereas the {111} facets on the C₇₀₅ particle contain a total of 96 possible adsorption sites. Both particles have the same number of adsorption sites on their {100} facets.

On the other hand, we can see that in the ammonia environment chemisorption of N on the surfaces of nanodiamonds is also endothermic (Figure 3c and d). Similarly, {100} facets are the most favored surfaces in both C₇₀₅ and C₈₃₇ nanoparticles. It is interesting to see that the formation energy decreases with

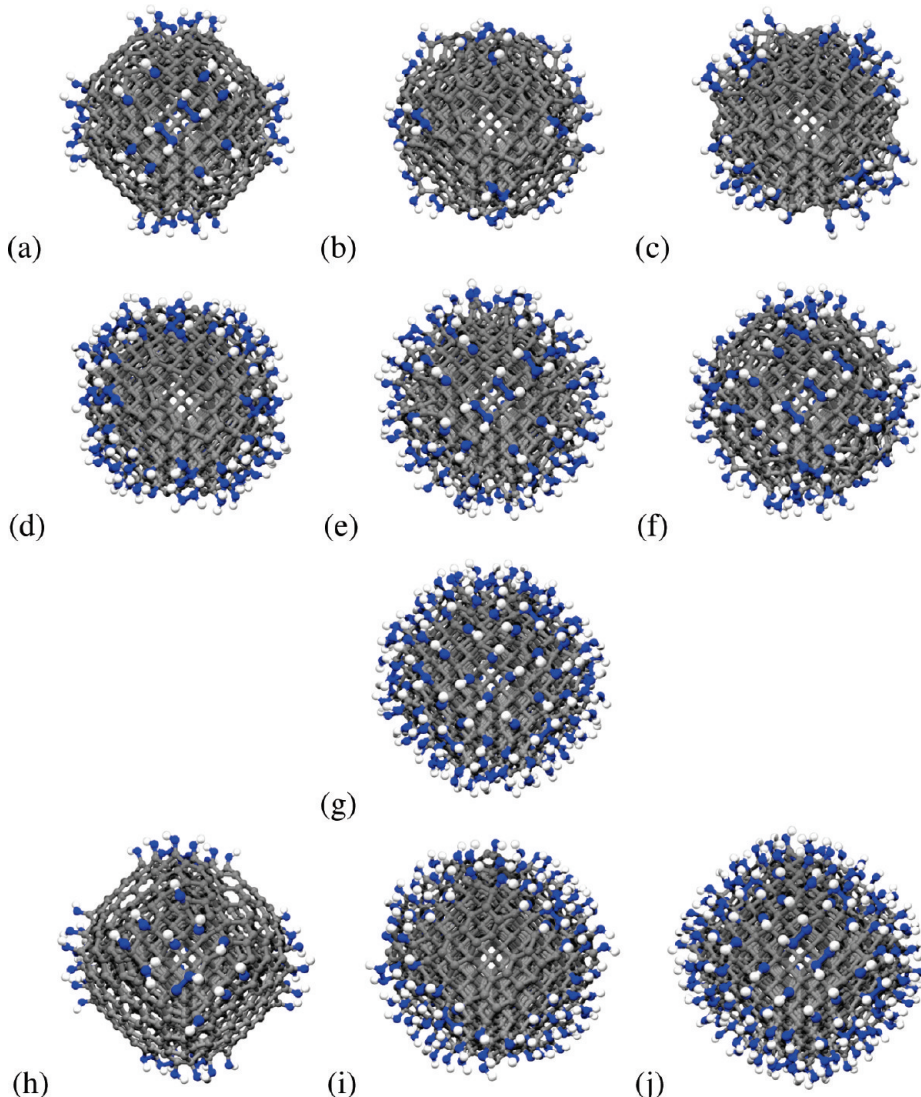


Figure 4. Fully relaxed structures for NH groups adsorbing on (a) {100} facets, (b) {110} facets, (c) {111} facets, (d) {110} and {111} facets ({100} clean), (e) {100} and {111} facets ({110} clean), (f) {100} and {110} facets ({111} clean), and (g) the entire surface of the C₇₀₅ nanodiamond, and on (h) {100} facets, (i) {111} facets, and (j) the entire surface of the C₈₃₇ nanodiamond. The blue, white, and gray balls denote the N atoms, H atoms, and C atoms, respectively.

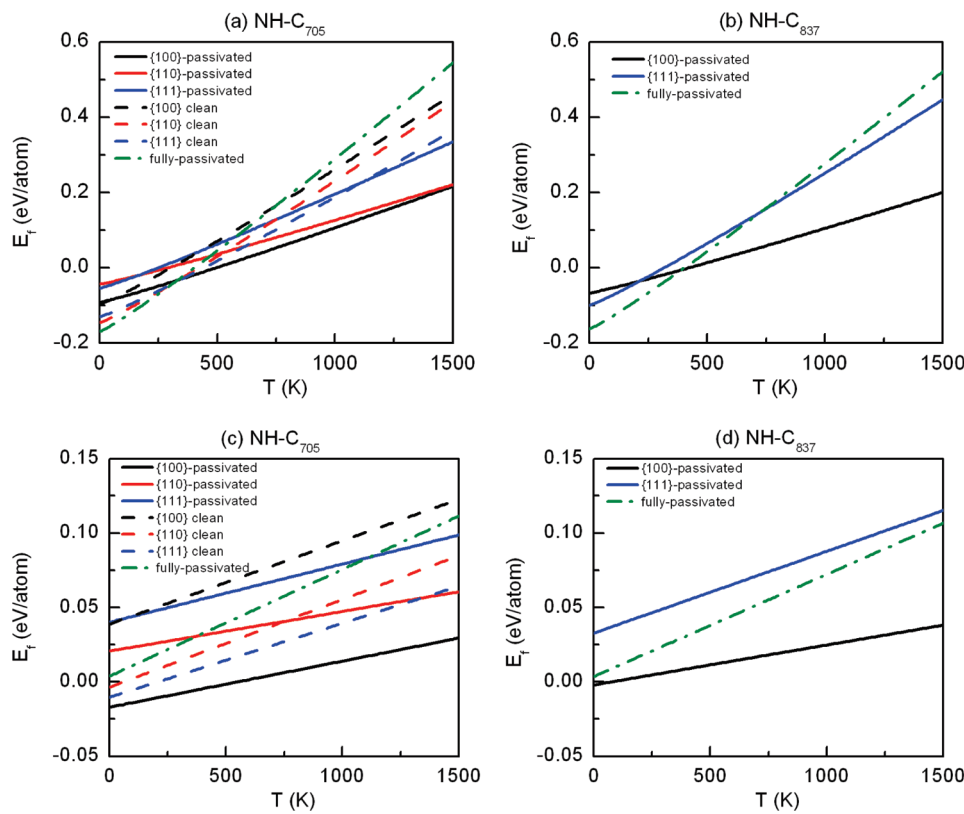


Figure 5. Formation energies in units of eV/atom, E_f , for C_{705} and C_{837} nanodiamonds with variant imidogen (NH) adsorption. Panels (a) and (b) are plotted with N_2 and H_2 as the reservoir while panels (c) and (d) with NH_3 as the reservoir.

increasing temperature. This is due to the higher bonding energy of N_2 , which requires more energy to break the N–N bonding and produce N-passivated nanodiamonds. As a result, passivation of N is more likely to occur and be more stable at high temperatures than at low temperatures. The fact that the stability decreases with increasing N coverage at low temperature (less than ~ 500 K in C_{705} nanoparticle) further confirms this explanation. Our results indicate that chemisorption is likely to occur at temperatures higher than ~ 1500 K. However, this critical temperature is too high to maintain the integral structure of the nanodiamond.

The adsorption energy for each configuration studied is presented in Table 2. We can see that adsorption of N is always endothermic on both C_{705} and C_{837} nanoparticles in either atmosphere or ammonia reservoir at $T = 0$, while the $\{100\}$ facets are energetically preferable surfaces for N adsorption.

The combination of the results shows that N is able to physically adsorb on nanodiamonds, and this interaction is preferable in the vicinity of the $\{100\}$ facets. Experimentally, either N atoms or nitrogen molecules that adsorbed on the nanodiamond surfaces can be easily removed through a heating treatment.

Imidogen Adsorption (NH). Simulation results for imidogen adsorption are shown in Figure 4, and the results of formation energies for NH-adsorbed C_{705} and C_{837} nanoparticles with respect to temperature are shown in Figure 5. In general, NH groups are able to chemisorb on surfaces of nanoparticles at temperatures lower than about 400–500 K. For the C_{705} nanodiamond at $T = 0$, NH groups prefer to adsorb on the $\{100\}$ facets rather than the $\{111\}$ and $\{110\}$ facets. We find that

the formation energies for more heavily passivated configurations depend more sensitively on the temperature than those where much more restrictive passivation is allowed. In contrast, on the C_{837} nanodiamond NH groups prefer to chemisorb on the $\{111\}$ facets rather than the $\{100\}$ facets at temperatures lower than ~ 200 K, and the $\{100\}$ facets only become energetically favorable above ~ 200 K.

While these results demonstrate that adsorption on different facets (and in different combinations) is energetically inequivalent (with, for example, the NH-saturated C_{705} nanodiamond with bare $\{100\}$ facets exhibiting less stability than those with bare $\{110\}$ or $\{111\}$ facets) in the entire temperature range considered (up to 1500 K), a critical event occurs at around room temperature. Below ~ 300 K simultaneous passivation of all facets is thermodynamically preferred, but as the temperature is increased above this point, NH groups on the $\{110\}$ facets start to be desorbed, quickly followed by those on the $\{111\}$ facets ~ 300 K. Beyond this point, chemisorption of NH groups on the $\{100\}$ facets is stable up to ~ 500 K. In the case of the C_{837} nanoparticle, the desorption process is slightly different from that of the C_{705} nanoparticle since the morphology, symmetry, and size of the C_{837} nanodiamond differ from the C_{705} nanodiamond (as mentioned above). In this case, the fully-NH-passivated C_{837} nanodiamond starts to lose NH groups on the $\{111\}$ facets at about $T = 390$ K and then to desorb NH groups on the $\{111\}$ facets at $T \sim 410$ K.

Similarly, in an ammonia environment the $\{100\}$ facets are the most favored surfaces in both C_{705} and C_{837} nanoparticles, though the critical temperatures are significantly different. It is ~ 550 K for the C_{705} nanoparticle and ~ 60 K for the C_{837}

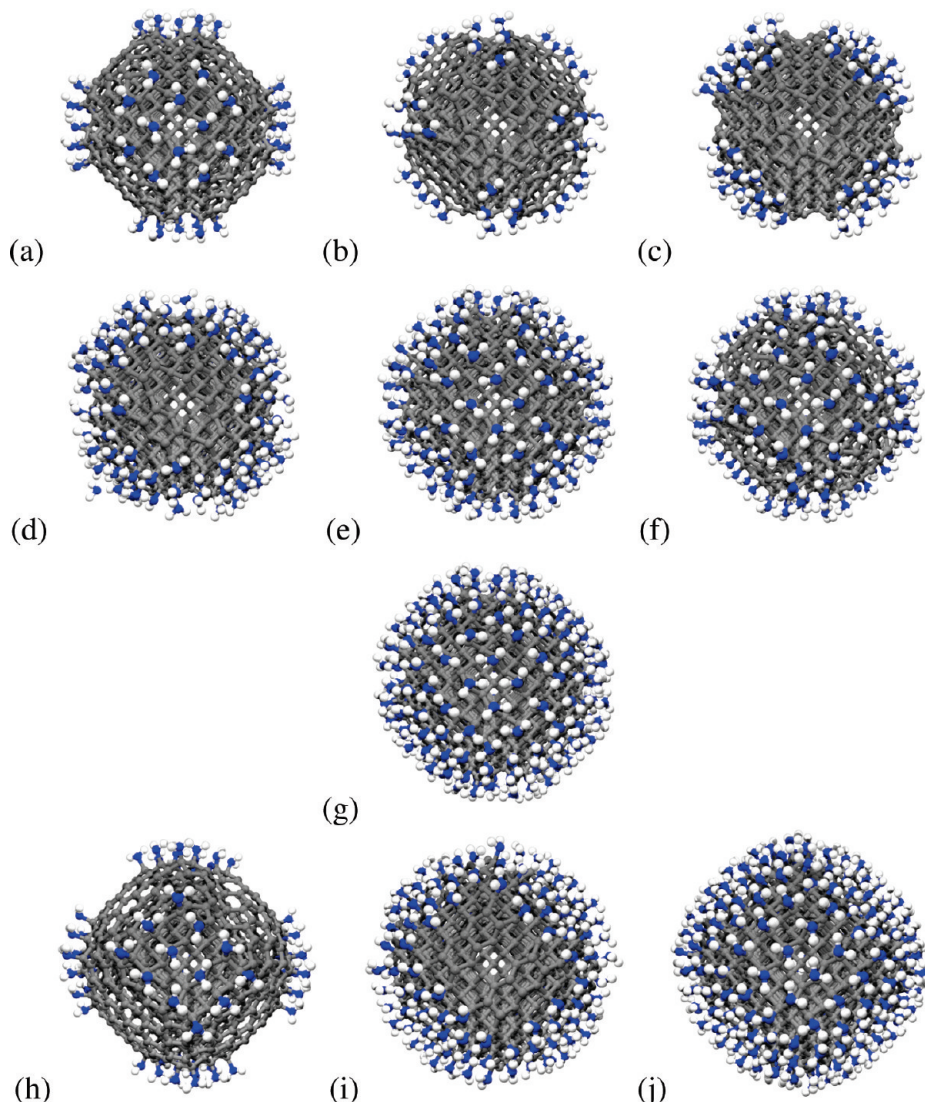


Figure 6. Fully relaxed structures for NH_2 groups adsorbing on (a) $\{100\}$ facets, (b) $\{110\}$ facets, (c) $\{111\}$ facets, (d) $\{110\}$ and $\{111\}$ facets ($\{100\}$ clean), (e) $\{100\}$ and $\{111\}$ facets ($\{110\}$ clean), (f) $\{100\}$ and $\{110\}$ facets ($\{111\}$ clean), and (g) the entire surface of the C_{705} nanodiamond and on (h) $\{100\}$ facets, (i) $\{111\}$ facets, and (j) the entire surface of the C_{837} nanodiamond. The blue, white, and gray balls denote the N atoms, H atoms, and C atoms, respectively.

nanoparticle where the desorption process starts. Generally, the NH -passivated C_{837} nanoparticle is less stable than the NH -passivated C_{705} nanoparticle with a higher formation energy (Figure 5c and d). In contrast to the $\text{N}_2 + \text{H}_2$ atmosphere, we can see that in an ammonia environment full passivation of both C_{705} and C_{837} nanoparticles by NH groups is endothermic in the temperature range considered (up to 1500 K). This suggests a route to selectively passivate nanodiamonds with NH groups by selecting proper reaction conditions.

It is shown in Table 2 that the $\{100\}$ facets are the most favorable surfaces for NH adsorption in C_{705} and C_{837} nanoparticles at $T = 0$. Generally, nanodiamonds in the $\text{N}_2 + \text{H}_2$ atmosphere are more reactive for adsorption than in an ammonia environment with a lower adsorption energy. The adsorption energy on the $\{100\}$ surface of the C_{705} nanodiamond is about 0.173 eV (both reservoirs) lower than that of the C_{837} nanodiamond, although there is an equal number of dangling C atoms (sites for adsorbate) on their $\{100\}$ facets. This indicates not only

that the adsorption sites but also that the surface shape, size, and symmetry will play an important role in the adsorption ability of nanodiamonds.

Amidogen Adsorption (NH_2). Simulation results for amidogen adsorption are shown in Figure 6, and the results of formation energies of NH_2 -adsorbed C_{705} and C_{837} nanoparticles with respect to temperature are plotted in Figure 7. Generally, chemisorption of NH_2 groups is exothermic on nanodiamond surfaces up to high temperatures. Among the configurations considered, adsorption of NH_2 groups on the $\{110\}$ facets of the C_{705} nanodiamond is the least favorable, and the $\{111\}$ facets are only slightly more preferred than the $\{100\}$ facets at $T = 0$ K (the difference in formation energy is 67 meV per atom). Like the NH -passivated particles, the formation energy of the C_{705} nanoparticle with NH_2 -passivated $\{111\}$ facets is more sensitive to changes in temperature than that with NH_2 -passivated $\{100\}$ facets, and when the temperature exceeds ~ 100 K, the $\{100\}$ facets become the most favorable surfaces for NH_2 adsorption.

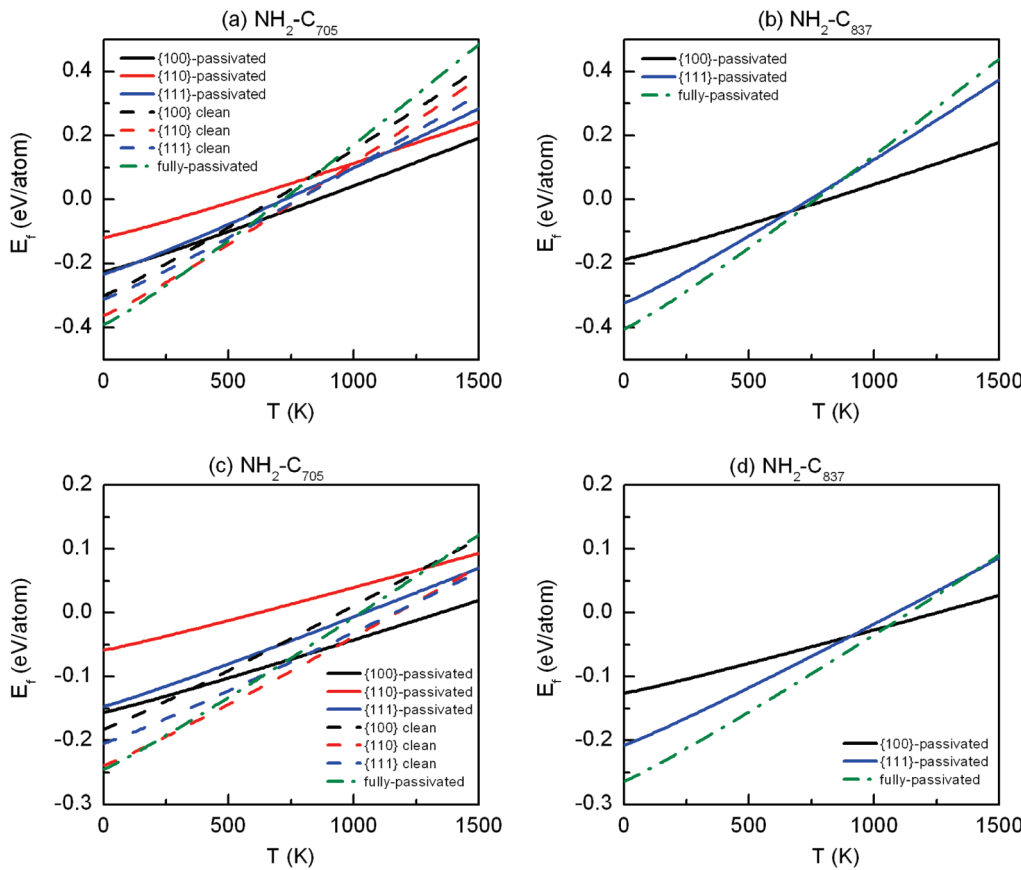


Figure 7. Formation energies in units of eV/atom, E_f , for C_{705} and C_{837} nanodiamonds with variant amidogen (NH_2) adsorption. Panels (a) and (b) are plotted with $N_2 + H_2$ as the reservoir while panels (c) and (d) with NH_3 as the reservoir.

This is consistent with results for other configurations, and we see that the NH_2 -adsorbed C_{705} nanoparticle with clean $\{100\}$ facets is slightly energetically less favorable than that with clean $\{111\}$ facets (and becomes more and more unfavorable with respect to an increase in temperature). Naturally we expect that the NH_2 -adsorbed C_{705} nanoparticle with clean $\{110\}$ facets is more stable than that with either clean $\{100\}$ or clean $\{111\}$ facets, as a larger number of sites are passivated. Overall, when the C_{705} nanoparticle is fully passivated, it is energetically stable at temperatures lower than ~ 350 K, at which point NH_2 groups desorb from the $\{110\}$ facets. As the temperature is increased up to ~ 700 K, the $\{111\}$ facets start to desorb NH_2 groups, and finally the NH_2 groups are entirely removed at about $T = 850$ K.

For the C_{837} nanoparticle the $\{111\}$ facets are energetically more favorable for NH_2 groups than the $\{100\}$ facets at low temperature. However, the critical temperature, above which the $\{111\}$ facets are less favorable than the $\{100\}$ facets for NH_2 adsorption, is about 660 K, which is much higher than that of the C_{705} nanoparticle.

It is found that both C_{705} and C_{837} nanoparticles can be readily functionalized with NH_2 groups at low temperatures. This indicates that, in practice, the nanodiamond stability and surface reactivity can be remarkably affected by NH_2 groups in the surrounding environment. It also suggests that one may use NH_2 groups to modify the surface properties or to improve the stability of the nanodiamond. We can see from Figure 7a that in a fully- NH_2 -saturated C_{705} nanoparticle it is the $\{110\}$ facets

that first desorb NH_2 groups at about $T = 300$ K as the temperature increases. Then NH_2 groups desorb from the $\{111\}$ facets at about $T = 700$ K, and finally they desorb from the $\{100\}$ facets at about $T = 850$ K. Similar to the C_{705} nanoparticle, when the temperature is increased, NH_2 groups desorb from the $\{111\}$ facets of the C_{837} nanoparticle at about $T = 720$ K and then from the $\{100\}$ facets at about $T = 800$ K.

Again in an ammonia environment we can see that the nanodiamond surfaces can readily accommodate full functionalization with NH_2 groups at low temperatures, although the corresponding formation energy ($T = 0$ K) is about 0.1–0.15 eV per atom higher than those in the $N_2 + H_2$ atmosphere. The fully- NH_2 -passivated C_{705} nanodiamond starts to desorb NH_2 groups from the $\{110\}$ surfaces quickly at ~ 200 K, then desorb from the $\{111\}$ surfaces at ~ 950 K, and finally from the $\{100\}$ surfaces at ~ 1350 K. For the C_{837} nanoparticle in an ammonia environment, it is the NH_2 groups on the $\{111\}$ surfaces that first desorb at ~ 1060 K, followed by the $\{100\}$ surfaces at ~ 1250 K. It is also found that the $\{100\}$ facets of the C_{705} nanodiamond are the most favored surfaces for NH_2 groups, while the $\{111\}$ facets of the C_{837} nanodiamond are energetically more favorable below ~ 900 K, above which the $\{111\}$ facets are less favorable than the $\{100\}$ facets for NH_2 adsorption.

As presented in Table 2 the nanodiamond exhibits a higher probability of NH_2 adsorption in a $N_2 + H_2$ environment than in an ammonia environment. Once again, the $\{100\}$ facets are found to be the most favored surfaces for this adsorbate. The fact that the adsorption energy on the $\{100\}$ facets of the C_{705}

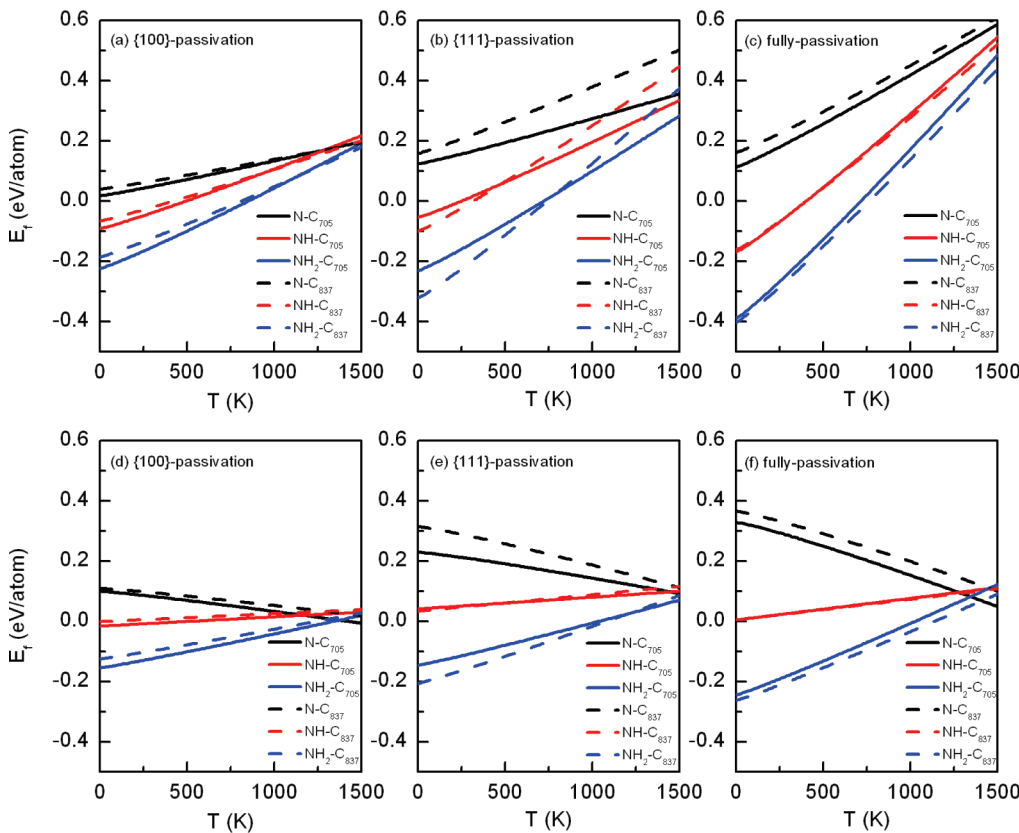


Figure 8. Stability comparison by formation energy (eV/atom) between C_{705} and C_{837} nanodiamonds with {111} facets, {100} facets, and the entire surface functionalized by N, NH, and NH_2 groups. Panels (a), (b), and (c) are plotted with respect to $N_2 + H_2$, while panels (d), (e), and (f) are with respect to ammonia (NH_3).

nanodiamond is about 0.151 (in $N_2 + H_2$) and 0.152 (in ammonia) eV lower than that of the C_{837} nanodiamond confirms the conclusion at the end of the imidogen adsorption section. It is also found that NH_2 is the most favored adsorbate for surface functionalization of nanodiamonds overall followed by NH.

Comparison. As mentioned above, it is straightforward to compare adsorption activity of N, NH, and NH_2 adsorbates due to the thermodynamic equilibrium condition invoked by eq 2. We can see from Figure 8 that C_{705} and C_{837} nanoparticles, representing rhombitruncated cuboctahedral and truncated octahedral bucky diamonds, can be entirely functionalized with NH and NH_2 groups, which form stable covalent chemical bonds at low temperatures. In general, the NH_2 groups are energetically more favorable than NH groups for complete monolayer functionalization within the typical temperature range (less than 1500 K). Singular N atoms are the least stable adsorbate and prefer to physisorb on the surface of nanodiamonds. In rare cases chemisorption may be achieved, but a modest heat treatment will undoubtedly remove these adsorbed N atoms. On the other hand, NH and NH_2 groups are desorbed from certain facets at different temperatures but are generally stable at room temperature.

To characterize the size dependence in these systems, we compare the formation energy (with respect to temperature) on like-facets of each structure in Figure 8. This comparison shows that there is very little difference in formation energies for fully passivated C_{705} and C_{837} nanoparticles, but when functionalization is restricted to certain facets, a slight difference in formation energies between C_{705} and C_{837} nanodiamonds can be discerned. This is attributed to differences in the surface morphology between

the two nanodiamonds. The presence of the {110} facets simultaneously introduces additional high-energy surfaces on the C_{705} particle but removes the highly strained {111}|{111} edges of the C_{837} structure and gives rise to different numbers of possible adsorption sites on the {111} facets of each structure. Beyond this observation, we can see that (in general) the results of amine adsorption are largely independent of particle size, thereby verifying that the assumed correspondence with the experimental measurements (above, on 500 nm particles) is valid.

In contrast, it is found that in a NH_3 reservoir N-adsorbed nanoparticles have an inversely proportional relationship with respect to temperature. It is also found that functionalization of the nanodiamond from a NH_3 reservoir is generally less stable than from a $N_2 + H_2$ reservoir. This suggests that N, NH, and NH_2 adsorbates on nanodiamond surfaces are more likely introduced when nanoparticles are exposed to air. In addition, functionalization in an artificial $N_2 + H_2$ atmosphere is more stable than that formed in an artificial NH_3 environment during a deliberate synthesis process.

In general, the stability of the NH-functionalized nanodiamond is very sensitive to the surrounding reservoir, far more so than the NH_2 -adsorbed nanodiamonds, as shown in Figure 8. We can see that complete monolayer passivation of nanodiamonds with NH is achievable in a $N_2 + H_2$ reservoir but is thermodynamically unstable in a NH_3 reservoir. In contrast, full NH_2 passivation is possible with both reservoirs.

It is important to point out that the NH groups on the C_{705} nanoparticle are entirely desorbed above ~ 500 K with an

atmosphere reservoir and ~ 550 K with an ammonia reservoir, while NH_2 groups on the C_{705} nanoparticle are entirely desorbed at ~ 850 K with an atmosphere reservoir and at ~ 1350 K with an ammonia reservoir. This implies that one may selectively functionalize nanodiamonds with NH_2 groups (irrespective of the reservoir) by choosing the proper reaction temperature. For instance, it may be possible to selectively passivate a rhombitruncated cubooctahedral nanoparticle, such as the C_{705} structure, with NH_2 groups, and perhaps NH groups, with temperatures in the range $550\text{--}800$ K in $\text{N}_2 + \text{H}_2$ and in the range $550\text{--}1350$ K in ammonia. Although these temperatures are in very good agreement with the experimental results for diamond surfaces, it is also noted that this temperature range is influenced by nanoparticle shape, size, and morphology, as described above.

CONCLUSIONS

In summary, we have examined the thermodynamic stability of partial (on specific facets) and full N , NH , and NH_2 functionalization of nanodiamonds by density functional tight binding simulations. The rhombitruncated cubooctahedral and truncated octahedral nanoparticles are modeled by the C_{705} and C_{837} nanodiamond structures, respectively, and the environmental influence is probed by using $\text{N}_2 + \text{H}_2$ and ammonia reservoirs. Our results show that the forced N-functionalization on nanodiamond surfaces is endothermic in a typical temperature range (lower than 1500 K) with either $\text{N}_2 + \text{H}_2$ or ammonia reservoirs. In contrast, both NH and NH_2 adsorption is energetically favored around room temperature in both reservoirs. However, the stability of these functionalized nanoparticles is greatly affected by the temperature and surrounding reservoirs and also the size, shape, and morphology of the nanoparticle. Importantly, our results suggest that it is likely to be possible to selectively functionalize nanodiamonds with NH_2 groups by controlling the desorption temperature.

Work is currently underway to determine how the stability of the nanodiamond is affected by oxygen-rich and carbon-rich environments, with the eventual aim of modeling the stability of nanodiamond in air.

ASSOCIATED CONTENT

S Supporting Information. Detailed analysis on the hybridization and bonding information of the fully relaxed structures of all of the functionalized nanodiamonds are presented here. This material is available free of charge via the Internet at <http://pubs.acs.org>.

AUTHOR INFORMATION

Corresponding Author

*E-mail: amanda.barnard@csiro.au.

ACKNOWLEDGMENT

L.L. is funded under the CSIRO OCE Postdoctoral Fellowship, and A.S.B is funded under the ARC QEII. Computational resources for this project have been supplied by the National Computing Infrastructure (NCI) national facility under MAS Grant q27. The authors would like to thank James Rabeau and Jana Say from Macquarie University.

REFERENCES

- (1) Shenderova, O.; Gruen, D. *Ultrananocrystalline Diamond*; William-Andrew: Norwich, NY, 2006.
- (2) Dolmatov, V. Y. *Rus. Chem. Rev.* **2001**, *70*, 607.
- (3) Danilenko, V. V. *Phys. Solid State* **2004**, *6*, 595.
- (4) Shenderova, O. A.; Zirnov, V. V.; Brenner, D. W. *Crit. Rev. Solid State Mater. Sci.* **2002**, *27*, 227.
- (5) Achatz, P.; Garrido, J. A.; Williams, O. A.; Bruno, P.; Gruen, D. M.; Kromka, A.; Steinmüller, D.; Stutzmann, M. *Phys. Status Solidi A* **2007**, *204*, 2874.
- (6) Hu, Y. H.; Shenderova, O. A.; Hu, Z.; Padgett, C. W.; Brenner, D. W. *Rep. Prog. Phys.* **2006**, *69*, 1847.
- (7) Chao, J.-I.; Perevedentseva, E.; Chung, P.-H.; Liu, K.-K.; Cheng, C.-Y.; Chang, C.-C.; Cheng, C.-L. *Biophys. J.* **2007**, *93*, 2199.
- (8) Schrand, A. M.; Hens, S. A. C.; Shenderova, O. A. *Crit. Rev. Solid State Mater. Sci.* **2009**, *34*, 18.
- (9) Dement'ev, A. P.; Maslakov, K. I. *Phys. Solid State* **2004**, *46*, 678–680.
- (10) Osawa, E. *Diamond Relat. Mater.* **2007**, *16*, 2018–2022.
- (11) Krueger, A. *Adv. Mater.* **2008**, *20*, 2445.
- (12) Fang, X.-W.; Mao, J.-D.; Levin, E. M.; Schmidt-Rohr, K. *J. Am. Chem. Soc.* **2009**, *131*, 1426–1435.
- (13) Kuznetsov, V. L.; Chuvilin, A. L.; Butenko, Y. V. *Chem. Phys. Lett.* **1994**, *222*, 343–348.
- (14) Banhart, F. *Rep. Prog. Phys.* **1999**, *62*, 1181.
- (15) Barnard, A. S.; Sternberg, M. *J. Mater. Chem.* **2007**, *17*, 4811.
- (16) Iakoubovskii, K.; Baidakova, M. V.; Wouters, B. H.; Stesmans, A.; Adriaenssens, G. J.; Vul', A. Y.; Grobet, P. J. *Diamond Relat. Mater.* **2000**, *9*, 861–865.
- (17) Mainwood, A. *Phys. Rev. B* **1994**, *49*, 7934.
- (18) Goss, J. P.; Briddon, P. R.; Rayson, M. J.; Sque, S. J.; Jones, R. *Phys. Rev. B* **2005**, *72*, 035214.
- (19) Rabeau, J. R.; Stacey, A.; Rabeau, A.; Prawer, S.; Jelezko, F.; Mirza, I.; Wrachtrup, J. *Nano Lett.* **2007**, *7*, 3433–3437.
- (20) Vlasov, I. I.; Barnard, A. S.; Ralchenko, V. G.; Lebedev, O. I.; Kanazuba, M. V.; Saveliev, A. V.; Konov, V. I.; Goovaerts, E. *Adv. Mater.* **2008**, *21*, 808.
- (21) Barnard, A. S.; Vlasov, I. I.; Ralchenko, V. G. *J. Mater. Chem.* **2009**, *19*, 360.
- (22) Iakoubovskii, K.; Adriaenssens, G. J. *Diamond Relat. Mater.* **2000**, *9*, 1349.
- (23) Vlasov, I. I.; Shenderova, O.; Turner, S.; Lebedev, O. I.; Basov, A. A.; Sildos, I.; Rähn, M.; Shiryaev, A. A.; Tendeloo, G. V. *Small* **2010**, *6*, 687–694.
- (24) Schrand, A. M.; Huang, H. J.; Carlson, C.; Schlager, J. J.; Osawa, E.; Hussain, S. M.; Dai, L. *J. Phys. Chem. B* **2007**, *111*, 2–7.
- (25) Chao, J. I.; Liu, K. K.; Cheng, C. L.; Chang, C. C. *FASEB J.* **2007**, *21*, A267–A267.
- (26) Barnard, A. S. *Analyst* **2009**, *134*, 1751–1764.
- (27) Fu, C.-C.; Lee, H.-Y.; Chen, K.; Lim, T.-S.; Wu, H.-Y.; Lin, P.-K.; Wei, P.-K.; Tsao, P.-H.; Chang, H.-C.; Fann, W. *Proc. Nat. Acad. Sci. U.S.A.* **2007**, *104*, 727.
- (28) Chang, Y.-R.; Lee, H.-Y.; Chen, K.; Chang, C.-C.; Tsai, D.-S.; Fu, C.-C.; Lim, T.-S.; Tzeng, Y.-K.; Fang, C.-Y.; Han, C.-C.; Chang, H.-C.; Fann, W. *Nat. Nanotech.* **2008**, *3*, 284.
- (29) Chen, M.; Pierstorff, E. D.; Lam, R.; Li, S. Y.; Huang, H.; Osawa, E.; Ho, D. *ACS Nano* **2009**, *3*, 2016–2022.
- (30) *Nanodiamonds: Applications in Biology and Nanoscale Medicine*; Ho, D., Ed.; Springer Science + Business Media: New York, 2009.
- (31) Barnard, A. S.; Sternberg, M. *J. Phys. Chem. B* **2005**, *109*, 17107.
- (32) Goss, J. P.; Briddon, P. R.; Papagiannidis, S.; Jones, R. *Phys. Rev. B* **2004**, *70*, 235208.
- (33) Barnard, A. S.; Sternberg, M. *Nanotechnology* **2007**, *18*, 025702.
- (34) Barnard, A. S.; Sternberg, M. *Diamond Relat. Mater.* **2007**, *16*, 2078.
- (35) Bradac, C.; Gaebel, T.; Naidoo, N.; Rabeau, J. R.; Barnard, A. S. *Nano Lett.* **2009**, *9*, 3555–3564.

- (36) Raty, J. Y.; Galli, G.; Bostedt, C.; van Buuren, T. W.; Terminello, L. J. *Phys. Rev. Lett.* **2003**, *90*, 37402.
- (37) Barnard, A. S.; Russo, S. P.; Snook, I. K. *Phys. Rev. B* **2003**, *68*, 73406.
- (38) Bradac, C.; Gaebel, T.; Naidoo, N. N.; Sellars, M. J.; Twamley, J.; Brown, L.; Barnard, A. S.; Plakhotnik, T.; Zvyagin, A. V.; Rabeau, J. R. *Nat. Nanotech.* **2010**, *5*, 345–349.
- (39) Liu, Y.; Gu, Z.; Margrave, J. L.; Khabashesku, V. N. *Chem. Mater.* **2004**, *16*, 3924–3930.
- (40) Yeap, W. S.; Tan, Y. Y.; Loh, P. *Anal. Chem.* **2008**, *80*, 4659–4665.
- (41) Dahoumane, S. A.; Nguyen, M. N.; Thorel, A.; Boudou, J.-P.; Chehimi, M. M.; Mangeney, C. *Langmuir* **2009**, *25*, 9633–9638.
- (42) Miller, J. B.; Brown, D. W. *Langmuir* **1996**, *12*, 5809–5817.
- (43) Chung, P.-H.; Perevedentseva, E.; Tu, J.-S.; Chang, C.; Cheng, C.-L. *Diamond Relat. Mater.* **2006**, *15*, 622–625.
- (44) Krüger, A.; Liang, Y.; Jarre, G.; Stegk, J. *J. Mater. Chem.* **2006**, *16*, 2322–2328.
- (45) Spitsyn, B. V.; Davidson, J. L.; Gradoboev, M. N.; Galushko, T. B.; Serebryakova, N.; Karpukhina, T. A.; Kulakova, I. I.; Melnik, N. N. *Diamond Relat. Mater.* **2004**, *15*, 296–299.
- (46) Hens, S.; Cunningham, G.; Tyler, T.; Mosseenkov, S.; Kuznetsov, V.; Shenderova, O. *Diamond. Relat. Mater.* **2008**, *17*, 1858–1866.
- (47) Huang, L.-C.; Chang, H.-C. *Langmuir* **2004**, *20*, 5879–5884.
- (48) Purtov, K. V.; Petunin, A. I.; Burov, A. E.; Puzyr, A. P.; Bondar, V. *Nanoscale Res. Lett.* **2010**, *5*, 631–636.
- (49) Miller, J. B. *Surf. Sci.* **1999**, *439*, 21.
- (50) Zhang, X.-Q.; Chen, M.; Lam, R.; Xu, X.; Osawa, E.; Ho, D. *ACS Nano* **2009**, *3*, 2609–2616.
- (51) Porezag, D.; Frauenheim, T.; Köhler, T.; Seifert, G.; Kaschner, R. *Phys. Rev. B* **1995**, *51*, 12947.
- (52) Frauenheim, T.; Seifert, G.; Elstner, M.; Niehaus, T.; Köhler, C.; Amkreutz, M.; Sternberg, M.; Hajnal, Z.; Carlo, A. D.; Suhai, S. *J. Phys.: Condens. Matter* **2002**, *14*, 3015.
- (53) Barnard, A. S. *J. Mater. Chem.* **2008**, *18*, 4038.
- (54) Li, W. F.; Irle, S.; Witek, H. A. *ACS Nano* **2010**, *4*, 4475–4486.
- (55) <http://www.dftb.org/parameters/download/>.
- (56) Kohler, C.; Frauenheim, T. *Surf. Sci.* **2006**, *600*, 453–460.
- (57) Barin, I. *Thermochemical Data of Pure Substance*; VCH Publishers, Inc.: New York, NY, 2006.